FT-IR Measurements of Atmospheric Trace Gases and their Fluxes

David W.T. Griffith

Reproduced from:

Handbook of Vibrational Spectroscopy

John M. Chalmers and Peter R. Griffiths (Editors)

FT-IR Measurements of Atmospheric Trace Gases and their Fluxes

David W.T. Griffith
University of Wollongong, Wollongong, Australia

1 INTRODUCTION AND SCOPE

Changing atmospheric composition is the primary driving force behind most aspects of global climate change. Increasing concentrations of radiatively active ("greenhouse") gases such as CO_2, CH_4 and N_2O in the troposphere and ozone depleting gases such as nitrogen oxides and chlorofluorocarbons in the stratosphere are well established.[1] Atmospheric composition needs constant monitoring and a much better understanding of the sources and sinks of critical trace gas species is required to understand their global budgets if we are to make well-informed decisions on strategies and international protocols for their control. In this chapter, we focus on Fourier transform infrared (FT-IR) measurement techniques for four of the most abundant and important trace gases – CO_2, CH_4, N_2O and CO. Current understanding of the global budgets of these compounds has been summarized recently by the Intergovernmental Panel on Climate Change.[1] CO_2 is the dominant greenhouse gas in the atmosphere (after water vapor); its atmospheric mixing ratio has increased from less than 300 ppmv (μmol mol^{-1}) to nearly 360 ppmv in the past century. CO_2 accounts for about 60% of global radiative forcing, and large fluxes of CO_2 occur through respiration and photosynthesis over all land surfaces, while the oceans are an important sink. CH_4, with a mean atmospheric mixing ratio of around 1.7 ppmv increasing at 0.5% per year, provides about 20% of radiative forcing, and N_2O, 310 ppbv (nmol mol^{-1}) increasing at 0.2% per annum, provides 8%. N_2O is also the dominant source of nitric oxide (NO) in the stratosphere where it is a principal catalyst in ozone destruction. For CH_4 and N_2O all sources are located at the earth's surface and are mostly biogenic in origin. In both cases the dominant sinks are through atmospheric photochemistry, but globally 5–10% of CH_4 is also thought to be destroyed in soils. Anthropogenic sources dominate natural sources, roughly 70% and 50% for CH_4 and N_2O, respectively, but source strength estimates have large uncertainties, especially for N_2O. Much of this uncertainty comes about because the sources are widely distributed, with small areal fluxes distributed over large areas leading to large gross fluxes presenting a difficult measurement challenge.

Simpler, cheaper and better techniques for measuring atmospheric composition and trace gas fluxes are highly desirable, and infrared (IR) spectroscopy has much to offer. Several articles in this Handbook describe applications to industrial gas emissions (see **Open-path Fourier Transform Infrared Spectroscopy**), emissions from biomass burning (see **Vibrational Spectroscopy in the Study of Fires**) and astronomical applications (see **Astronomical Vibrational Spectroscopy**), as well as the use of long path cells (see **Long Path Gas Cells**) and IR emission measurements (see **Passive Remote Sensing by FT-IR Spectroscopy**). A recent review[2] gives an overview of many of these applications. In this article we focus on two themes: applications of FT-IR spectrometry for high precision in situ measurements of CO_2, CH_4, N_2O and CO in relatively clean air, and remote sensing of atmospheric composition by ground-based high resolution solar FT-IR spectroscopy. Portable instruments and methods suited to field measurements of trace gas composition are described in Section 2. Section 3 describes several approaches to the measurement of rates of emission and exchange of these trace gases with sources and sinks at the earth's surface. Ground-based remote sensing is described in Section 4.

2 IN SITU AND SAMPLING METHODS

The methods described are based on FT-IR absorption spectrometry using multiple-reflection gas cells to achieve high precision and accuracy at natural clean air levels. They are suited to measurements of CO_2, CO, CH_4 and N_2O, as well as to natural variations in the $^{13}CO_2/^{12}CO_2$ ratio. In this section we describe two variations of the equipment as well as methods for quantitative analysis.

2.1 Single beam spectrometer

The simplest implementation is illustrated schematically in Figure 1 and described in detail by Esler *et al.*[3,4] The instrument is based on a standard Bomem MB100-series FT-IR spectrometer at $1\,cm^{-1}$ resolution fitted with standard globar source and either KBr or ZnSe beamsplitter. CO_2, CO, CH_4, N_2O, $^{13}CO_2$ and water vapor all have strong and suitable absorption bands above $2000\,cm^{-1}$, allowing the use of a liquid nitrogen-cooled indium antimonide (InSb) detector. InSb detectors provide background-limited noise performance and maximum detectivity, but only at frequencies above $1800\,cm^{-1}$. For other species such as NH_3, a mercury cadmium telluride (MCT) detector is required to cover the $700–1300\,cm^{-1}$ spectral region. To obtain sufficient precision for trace gases at clean air background mixing ratios, an absorption pathlength of around 10 m or more is required; we have used closed multi-pass cells of 10–100 m total pathlength following the designs of White[5,6] or Horn and Pimentel[7] and described elsewhere in this Handbook (**Long Path Gas Cells**). The spectrometer and cell are enclosed in a temperature-controlled, purged enclosure to avoid temperature-dependent effects on calibration and interference from the ambient atmosphere, particularly CO_2. The spectrometer cell is filled and evacuated through a manifold of solenoid valves, and the pressure and temperature of the sample cell are routinely measured. Automated solenoid valve control and pressure/temperature logging are performed by a standard data acquisition and digital I/O control card in the controlling PC. A single computer program fully automates all aspects of operation in real time – sample handling, spectrometer operation and data acquisition, temperature and pressure logging, quantitative analysis of the spectra, and output of results. For Bomem spectrometers operating in the Grams environment (Galactic Industries Inc.) all programs are written in the Galactic Array Basic language. The actual sample handling protocol varies between applications but is easily configured by the sampling manifold design and controlling program. We have used this system for ambient air monitoring, continuous flux chamber measurements and automated sample flask analysis.

This combination of hardware provides signal-to-noise ratios (S/N) of the order of 50 000 root mean square (rms) in a single beam spectrum for a 10 min coadding time (256 single scans). In general we find that the S/N decreases at shorter scan times following the theoretical square root law, and that the quantitative precision obtained decreases proportionally with the S/N. However for longer scan times

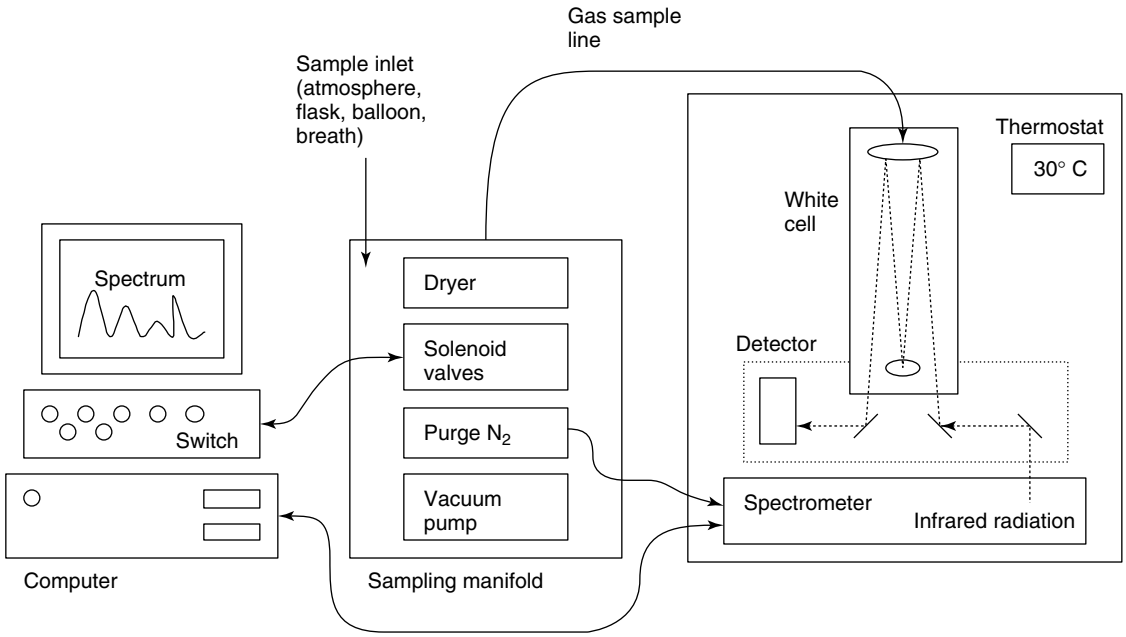

Figure 1. Schematic diagram of single beam FT-IR spectrometer and cell. [Reproduced by permission of the American Chemical Society, from Esler *et al.* (2000).[3]]

slow drifts in the overall response and 100% level limit the quantitative precision, and scan times of 10–20 min are optimal for best precision. Precision and accuracy obtainable with this system is described in Section 2.4.

2.2 Dual beam spectrometer

For micrometeorological applications the time available for real-time atmospheric analysis is limited and there is a trade-off between analytical precision and measurement time. A dual beam spectrometer with two matching sample cells effectively doubles the duty cycle of the spectrometer: either two sample lines can be analyzed almost simultaneously, or one sample can be prepared in one cell while the other is being analyzed. We have used such a dual beam FT-IR spectrometer in a number of micrometeorological applications described below. The dual beam instrument is described by Griffith and Galle[8] and Griffith *et al*.,[9] and is based on the Bomem MB100 corner-cube interferometer which allows simultaneous access to the two output beams of the interferometer from a single source input beam. The spectrometer is shown schematically in Figure 2. The two output beams of the interferometer are directed through shutters and matched 57-m multipass cells, then brought parallel and combined by a parabolic mirror onto a single InSb detector. A similar sample manifold, controlling computer and program to that described above is used; in addition, either or both FT-IR beams can be selected by opening and closing the appropriate shutters. In one mode of operation,[8] continuous flows of air from two sample lines through the two cells are analyzed pseudo-simultaneously by switching shutters every few seconds and averaging spectra over a time period, typically 20–30 min for micrometeorological applications. In a second mode,[9] air samples are analyzed alternately; one cell is evacuated and refilled from the manifold while the spectrum of the other is being measured by the FT-IR spectrometer.

This dual beam configuration also allows a true differential measurement between the two cells directly by optical subtraction.[8] The interferograms from the two output beams are out of phase with each other, and if both shutters are simultaneously open, the combined interferogram at the detector is that of the difference between the two beams. This is attractive in principle for true differential measurements between similar samples, but in practice we have found it difficult to maintain sufficient alignment stability of the dual beam spectrometer so that the theoretical advantages over single beam measurements can be realized.

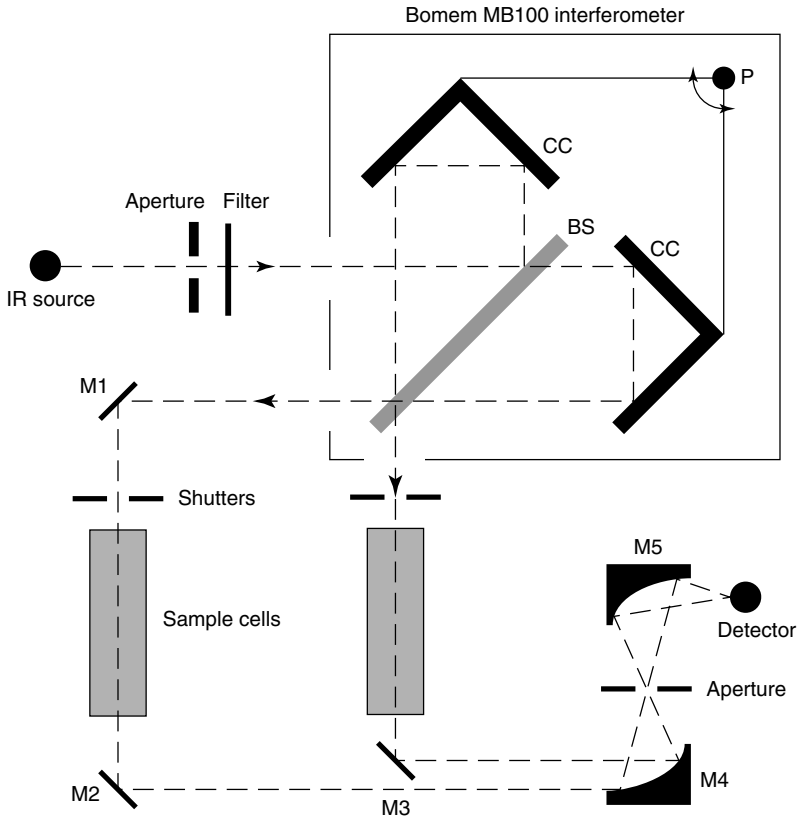

Figure 2. Schematic diagram of a dual beam FT-IR spectrometer. [Reproduced by permission of Elsevier Science Ltd., from Griffith and Galle (2000).[8]]

2.3 Quantitative analysis

Air is a multicomponent mixture; simultaneous determination of multiple species with good precision and accuracy requires careful attention to calibration and quantitative analysis. These may be considered in two parts – firstly the generation of reference spectra in which the composition of absorbing species is well known, and secondly the method by which the spectra are quantitatively analyzed.

2.3.1 Generation of reference or calibration spectra

In clean air at pathlengths up to 100 m, the dominant absorbers in the mid-infrared are H_2O (0–3%), CO_2 (360 ppmv), CH_4 (1.7 ppmv), N_2O (310 ppbv) and CO (50–100 ppbv). At normal atmospheric pressure, individual rotational–vibrational linewidths are of the order of $0.1\,cm^{-1}$, and except for N_2O individual lines are resolved at $1\,cm^{-1}$ spectral resolution. There can therefore be significant deviations from Beer's Law for all but the weakest absorption.[10–12] For best precision a simple linear response between absorbance and concentration, independent for each component, cannot be generally assumed, and pure single component spectra are not an appropriate basis for calibration. Reference spectra should ideally be obtained with all components varied over the expected concentration ranges, under the same environmental conditions as pertain to the measured unknown spectra. Clearly this is a demanding and time consuming task, especially if environmental conditions, sample concentration ranges or spectrometer alignment are subject to changes. For open path measurements, it is impossible to create such reference spectra over the sample path.

To simplify this task, our approach has been to calculate reference or calibration spectra using a computer program MALT, described in detail by Griffith.[13] Starting from a database of absorption line parameters such as HITRAN,[14] the monochromatic absorptivity spectra or optical depths, $\tau(\nu)$, are calculated for each component by convolution of a set of delta functions defined by the line parameter database with the pressure (Lorentzian) and Doppler (Gaussian) broadening lineshape contributions for each absorption line, followed by scaling for the amount of each component. Individual isotopic species such as $^{13}CO_2$ and $^{12}CO_2$ can be treated as separate species and analyzed individually for isotopic fractionation studies. The absorptivities are summed at each wavenumber to obtain the total monochromatic spectrum. This summation is strictly linear, and is therefore accurate for any component concentrations. The monochromatic transmission spectrum of a sample of absorptivity $\tau(\nu)$ is $T(\nu) = e^{-\tau(\nu)}$. $T(\nu)$ is convolved with the instrument lineshape function (ILS), which in an ideal spectrometer has contributions from the instrument resolution, apodizing function and field of view (divergence) of the beam in the interferometer. This convolution is not linear in the component concentrations and is the source of non-Beer's-law behavior at low spectral resolution. The ILS contributions are well understood and can be calculated exactly,[15,16] and the resulting spectra faithfully reproduce spectra which would be observed from an ideal FT-IR spectrometer. Misalignment of the spectrometer (off-axis or off-focus collimator apertures[17,18]) as well as uncorrected phase errors can also be modeled in the ILS to better match real measured spectra. In the following steps, we use calculated spectra in place of measured spectra for the purposes of calibration and quantitative analysis.

2.3.2 Quantitative determination of trace gases from spectra

A more comprehensive overview of quantitative analysis methods for FT-IR atmospheric trace gas analysis is given by Griffith and Jamie.[2] The simplest approach is to use traditional peak height or peak area analysis, using calculated calibration spectra to construct absorbance–concentration calibration curves from suitably isolated absorption features. However multivariate full spectrum methods such as Classical Least Squares (CLS) or Partial Least Squares (PLS) generally provide better precision, accuracy and reliability because they use more of the available spectral information.[19] Less easily available, but more powerful and flexible, are nonlinear least squares (NLLS) fitting methods in which measured spectra are fitted by iteratively re-calculating spectra until a least squares best fit is obtained. In what follows, we concentrate on CLS and NLLS methods.

In CLS,[19,20] a linear combination of single component reference spectra of the individual compounds is fitted to the measured spectrum such that the rms of the residuals at each wavenumber is minimized. The amounts of each absorber required in the best fit provide the required quantitative result. The equations for the regression can be readily written and solved in matrix form so that the method is computationally fast and efficient. The matrix of absorptivities is often called the K-matrix and CLS regression equivalently called the K-matrix method. Calibration in CLS is the determination of the basis set of single component spectra to be used in fitting the unknown spectra. The spectra can be measured as single pure component spectra or as mixtures (the "training spectra"), in which case a CLS calibration step is used to determine (again by least squares regression) the best single component spectra which fit the training set of calibration spectra. As discussed above, deviations from Beer's law must be considered when selecting calibration conditions and concentration ranges. In our approach, MALT is used to calculate the training

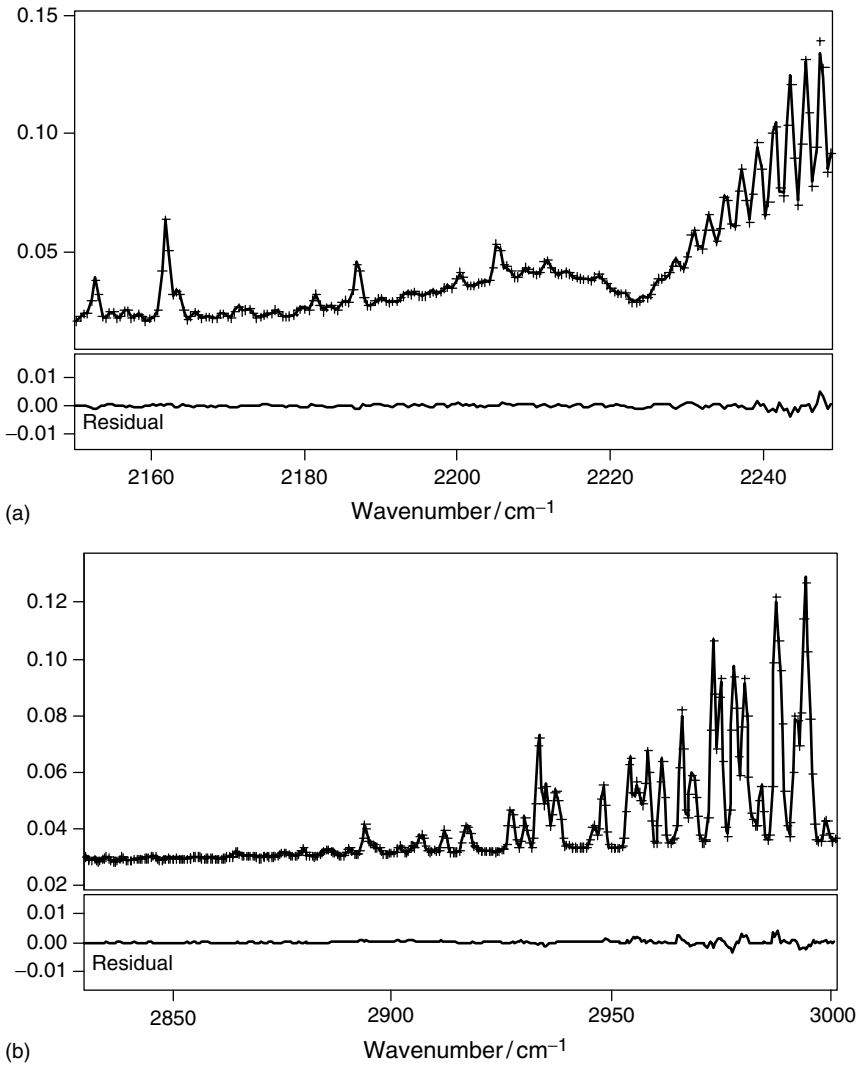

Figure 3. Examples of CLS fits of MALT-calculated spectra to measured spectra of undried clean air: (a) region used for CO_2, CO and N_2O analysis; and (b) region used for CH_4 analysis. −, measured; +, fitted.

spectra in place of actual measurements. The calculation of a set of 50 spectra takes only a few seconds, and the ILS parameters can be adjusted to get best fit to the measured unknown spectra. New sets of calibration spectra can be recalculated easily as required. Specific examples of the use of CLS in quantitative analysis are given in the applications described later in this article. Figure 3 illustrates typical CLS fits of MALT-calculated to measured spectra in two spectral regions used to determine CO_2, CH_4, N_2O and CO in undried air.

One well known drawback of CLS is that every absorbing component in a spectrum to be analyzed must be included in the calibration or the CLS algorithm will produce errors as it tries to fit absorption features which are not present in the calibration spectra. This is not generally a concern for clean air spectra at paths up to 100 m because all absorbers are normally known – they are H_2O, CO_2, CH_4, N_2O and CO. In heavily polluted air however the components should be known in advance and either included in the calibration model or added during the prediction phase.[21] Library reference spectra can also be included in the CLS model. PLS does not require a priori knowledge of the air composition, and with a suitable choice of training set based on libraries of spectra, PLS methods are able to avoid some of these limitations of CLS.

NLLS provides a different approach which, as the name implies, is not dependent on the linearity between absorbance and concentration inherent in Beer's law.[22,23] In NLLS, an initial guess is made at the unknown spectrum parameters, which may include for example component concentrations, ILS parameters and wavenumber scale shift. A spectrum is calculated for these parameters, for example by a program such as MALT, as well as the partial derivatives of the rms residual with respect to the fitting

parameters. The partial derivatives are used to make an improved estimate of the parameters, a new spectrum is calculated, and the process iterated until satisfactory fit (a predefined minimum rms residual) is obtained. The Levenberg–Marquart algorithm[24,25] is routinely used for efficient iteration and commonly available in software libraries. NLLS places no requirement of linearity on the parameters to be fitted, making it more flexible for general purpose spectrum fitting applications. Spectra are normally fitted as transmittance spectra because random noise levels are then constant at all ordinate values and all spectral points are equally weighted in the fit.

2.4 Precision and accuracy: calibration with gas standards

The precision and accuracy of FT-IR trace gas analysis are demonstrated by measurements of a suite of 11 clean air standards calibrated and maintained in high pressure tanks by CSIRO GASLAB in Melbourne Australia (http://www.dar.csiro.au/res/gac/ghg.htm).[26] The standards are used for calibration of instruments for the Australian clean air monitoring station at Cape Grim, Tasmania, and their calibration is traceable to primary gravimetric standards maintained by the US National Institute for Standards and Technology (NIST). In 1994, each of these tanks was analyzed using the single beam FT-IR system described in Section 2.1. The spectra were analyzed by CLS using MALT-calculated reference spectra, initially assuming the ideal ILS,[3,4] and later including a nonideal ILS in which misalignment and field of view were chosen to minimize the residuals between fitted and measured spectra.[27,28] The results are illustrated in Figure 4 and summarized in Table 1 for both the ideal and optimized ILS. In both cases the *precision* achieved (as measured by the SEP) is similar, of the order of 0.25% for CO_2, 0.1% for CH_4 and N_2O, and 0.5% for CO at atmospheric clean air background levels. The FT-IR results in Figure 4 and Table 1 are derived from the HITRAN database, MALT calculated spectra and CLS fitting, without any reference to calibration gases. The regressions thus indicate the absolute *accuracy* possible with the FT-IR method; with an optimized ILS, this accuracy is better than 1.5% for all four gases. The regressions are also highly linear – only in the case of CO is the regression improved significantly by adding a quadratic term. It is however well known that the gas chromatography/reduction gas detector analysis used to characterize CO in the suite of tanks has significant nonlinearities, and we believe that the observed curvature in the plots is due mostly to the assigned values, not the FT-IR determinations.

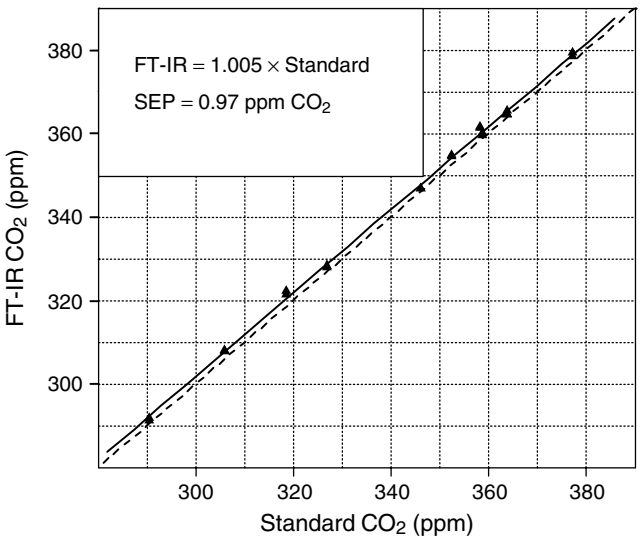

Figure 4. FT-IR determined vs assigned mixing ratios of CO_2 for a suite of clean air calibration standards. Similar analyses were made for CH_4, CO and N_2O and the results are summarized in Table 1.

Table 1. Regression statistics for determination of clean air standards by FT-IR against calibrated values. Slopes are given for regressions of FT-IR against assigned mixing ratios, as well as the standard error of prediction (SEP) from each regression.

Species	Accuracy		Precision (±%)
	Ideal ILS (%)	Nonideal ILS (%)	
CO_2	−1.0	0.5	0.25
CH_4	5.7	−1.5	0.1
N_2O	1.9	0.9	0.1
CO	−5.0	1.0	0.5

These results indicate the precision and accuracy achievable by FT-IR analysis, without the need for any calibration gases. Since the FT-IR response is highly linear, accuracy levels approaching those of the precision can be obtained when measuring unknown air samples by interleaving measurements of a standard gas of accurately known composition and using the apparent FT-IR determinations of this standard to correct determinations of unknowns.

3 APPLICATIONS

The techniques described in Section 2 provide a number of opportunities for novel and improved measurements of atmospheric trace composition and the rates at which trace gases are exchanged between the atmosphere and other reservoirs at the earth's surface. The applications described in this section have unique advantages deriving from the combination of good precision and accuracy of FT-IR analysis, the ability to determine several trace gases in a single

measurement, and full automation to allow continuous monitoring of composition and fluxes. Section 3.1 describes high precision monitoring of several trace gases simultaneously in clean air, while Sections 3.2–3.4 describe several FT-IR-based methods for trace gas flux measurements in agricultural, industrial and urban environments. Section 3.5 describes measurements of $^{13}CO_2$ isotopic fractionation during exchange with plants and soil in an agricultural environment.

3.1 Trace gas monitoring in clean air

The Australian Bureau of Meteorology operates a clean air background monitoring station at Cape Grim in NW Tasmania (40.7°S, 144.7°W) which is used for routine measurements of a wide range of atmospheric species using the most accurate and precise available instrumentation.[29] In 1995 we installed an automated single beam FT-IR spectrometer at Cape Grim and analyzed air samples every 30 min for 5 weeks.[3] Absolute calibration was accomplished by 6-hourly measurements of a single reference gas mixture of similar composition to clean air calibrated by CSIRO-GASLAB and similar to the suite of gases described in Section 2.4. Figure 5 shows time series of mixing ratios for CO_2, CH_4, N_2O and CO for the whole period, as well as for an extended period of baseline (clean air) conditions. The plots show measurements both by the single FT-IR instrument and by the dedicated analyzers for each species – nondispersive infrared (NDIR) for CO_2, and gas chromatography with flame ionization detection for CH_4, electron capture detection for N_2O and mercuric oxide reduction gas detection for CO.[29] In all cases, the results from the single FT-IR instrument agree within the observed scatter with the "standard" instruments with precisions of the order of those quoted in Table 1, which are at least as good as those provided by the individual instruments.

3.2 Micrometeorological measurements of surface–atmosphere trace gas exchange

Improved methods for quantifying the rates of surface–atmosphere exchange of trace gases are highly desirable to refine trace gas budgets, improve understanding of trace gas biogeochemical cycles, quantify sources of fugitive gas emissions, and underpin strategies for mitigation of trace gas emissions. We can distinguish three separate strategies for making such measurements:

- Chamber methods[30] have been and remain the most common for diffuse trace gas flux measurements from the earth's surface. In these methods a field chamber

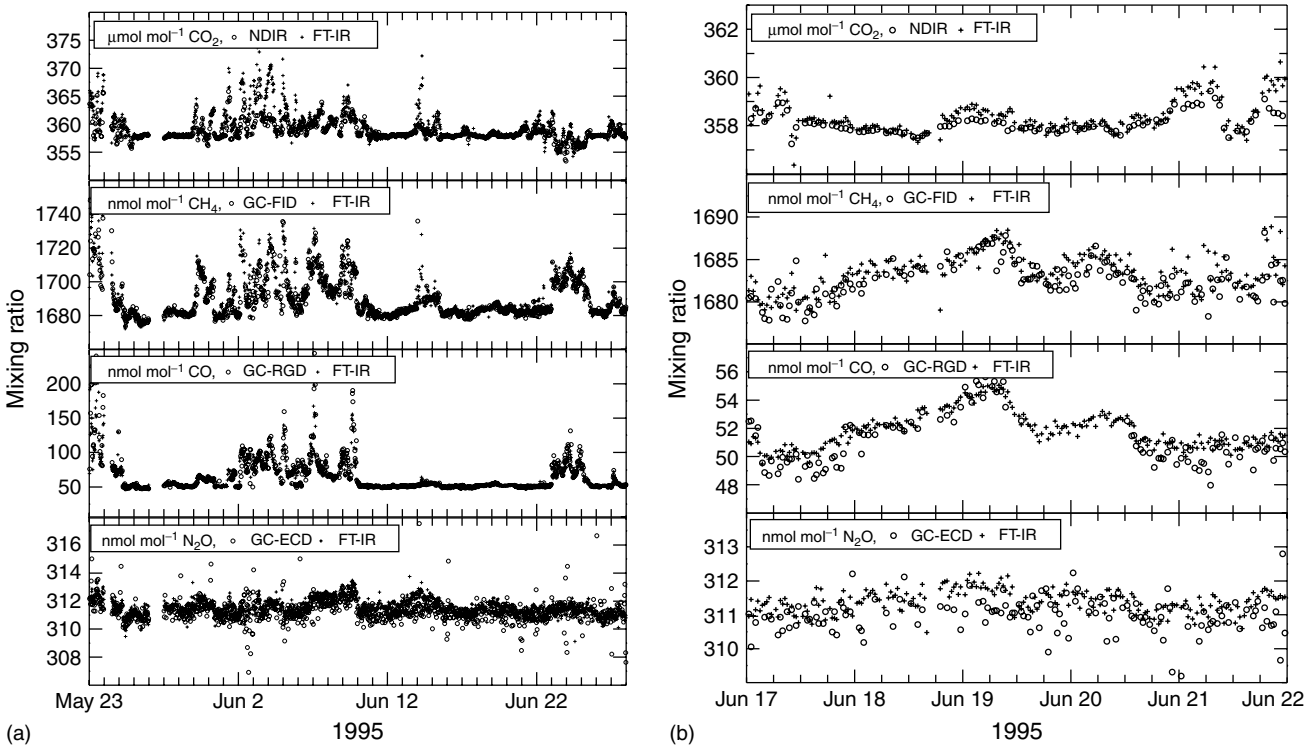

Figure 5. FT-IR, gas chromatography and NDIR measurements of trace gas mixing ratios at Cape Grim: (a) 23 May–28 June 1995; and (b) 17–22 June 1995 during an extended period of clean air conditions. [Reproduced by permission of the American Chemical Society, from Esler *et al*. (2000).[3]]

encloses a small surface area (typically $<1\,m^2$) and fluxes are determined by measurement of the rates of change of concentrations of trace gases in the chamber. They are the most sensitive and are relatively simple to implement, but suffer the important disadvantages that they sample only small areas and time spans (and therefore do not easily capture spatial and temporal variability), and may perturb the system being measured by changing the microclimate in the chambers.

- Micrometeorological methods such as eddy correlation, eddy accumulation and flux-gradient,[31] are by contrast nondisturbing, integrate over much larger areas (patch scale, typically $>10^4\,m^2$) and are more amenable to automation. Micrometeorological methods rely on measurements of atmospheric turbulence and eddy-diffusion rates combined with high precision trace gas concentration measurements. However these techniques are significantly harder and more restrictive to implement and place stringent requirements on trace gas analysis. For example for eddy correlation measurements, instruments must typically have 0.1-s response times to resolve small-scale turbulence, and for gradient flux or eddy accumulation measurements relative precision of the order of 0.1% is required to resolve small but significant fluxes.
- Tracer methods avoid some of the restrictions of both micrometeorological and chamber techniques. If a tracer gas is released at a known rate from points co-located with the sources of the trace gases of interest, simultaneous determination of tracer and fugitive source gas concentrations downwind allows direct calculation of the source gas release rate. Tracer methods are thus nonintrusive, but avoid some of the limitations of both chamber and micrometeorological techniques.

3.2.1 FT-IR flux gradient method

Figure 6 illustrates the principle of the flux gradient technique. Imagine a uniform surface exchanging a trace gas with the atmosphere, for example an agricultural crop releasing CO_2 at night time due to plant and soil respiration. If a steady wind blows across the surface, a steady-state concentration gradient will be established, decreasing upwards away from the surface source. During daytime, photosynthetic uptake at the surface will reverse the gradient. Provided there is no horizontal advection of the trace gas, mass balance requires that its vertical flux through any horizontal layer in the atmosphere above the surface be constant and equal to the flux at the surface. The principal mechanism for the vertical transport is diffusion, and the

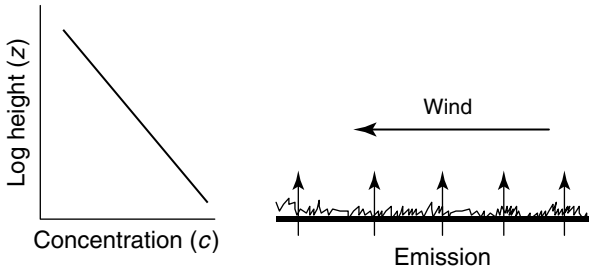

Figure 6. Schematic illustration of the flux-gradient technique. See text for details.

vertical flux is given by Fick's law,

$$F_x = -K\frac{dC_x}{dz} \tag{1}$$

where F_x is the flux of trace gas x, C_x its concentration, z the height above the surface and K the diffusion constant for the trace gas x in air. Turbulent or eddy diffusion normally dominates molecular diffusion and K is then the eddy diffusion constant, depending on atmospheric turbulence and stability. For further detail, see for example texts such as Monteith and Unsworth.[32]

Thus the determination of a trace gas exchange flux requires the determination of the vertical gradient of concentration and the diffusion constant K. The technique requires high precision (of the order of 0.1%) of trace gas concentration measurement, but not necessarily high accuracy. The eddy diffusion constant may be determined directly by fast (10 Hz) measurements of the vertical windspeed using a sonic anemometer, or from the vertical profile of wind speed. If the flux of a second trace gas can be measured independently, and its vertical concentration profile is also measured by the FT-IR spectrometer, K need not be determined explicitly and the flux of trace gas x can be calculated from

$$F_x = F_T\frac{dC_x}{dC_T} \tag{2}$$

where F_T and C_T are the directly measured flux and concentration of the second gas, and dC_x/dC_T is the slope of a regression of C_x vs C_T determined at different heights z. In effect, K is determined implicitly from F_T and dC_T/dz. Water vapor is a suitable second species since its flux can be routinely measured directly by eddy correlation and if the air stream to the FT-IR spectrometer is not dried, it is also routinely measured by the FT-IR spectrometer to determine its vertical gradient.

The combination of the flux gradient method with FT-IR spectrometry for trace gas determinations was first described for N_2O soil-flux measurements by Galle *et al.*[33] and has subsequently been applied to measurements of CO_2, CH_4, N_2O and NH_3 in various agricultural environments.[8,9,34,35] In October 1994 and 1995 we

participated in two large scale campaigns (OASIS[36]) to measure exchanges of energy, water vapor and trace gases in a heterogeneous rural environment in SE Australia.[9] During both OASIS campaigns we made continuous automated flux-gradient measurements of CO_2, N_2O and CH_4. Air was drawn continuously at 2–3 L min^{-1} from each of seven inlets at heights of 0.5, 1, 2, 4, 8, 14 and 22 m on a micrometeorological tower through 40-L buffer volumes to smooth out short-term fluctuations. Each sample line was analyzed twice on a 2-min measurement cycle to provide mean vertical profiles of CO_2, CH_4, N_2O, CO and H_2O every 30 min continuously for the 3 weeks of the campaign. Supporting measurements of wind speed, temperature and water vapor were made independently at each height, as well as eddy correlation measurements of heat, water vapor and CO_2 at 2 and 22 m. The FT-IR analysis was performed by a dual beam spectrometer as described above, using two 57-m Horn–Pimentel type cells (IR Analysis, Anaheim, CA), and was fully automated under control of an Array Basic program in the Grams operating environment. During each 2-min measurement period, one cell was evacuated and refilled with the next sample to be analyzed, while the spectrum of the sample in the other cell was recorded. Spectra were analyzed immediately after collection by CLS using a pre-calculated MALT-based calibration and allowed the measurements to be followed in real time.

Figure 7 shows typical vertical profiles of CO_2 from midnight to late morning, plotted as mixing ratio (horizontal axis) against ln(height) (vertical axis). Under ideal constant flux conditions, such plots should be straight lines.[32] During the night the surface is a CO_2 source due to plant and soil respiration, and there is both a strong negative gradient and a build up of CO_2 in the nocturnal boundary layer. Following sunrise at ca. 06 : 00, photosynthesis begins and there is a rapid drawdown of CO_2 and reversal of the negative gradient. Figure 8(a) shows the average diurnal variations of CO_2 over the campaign period. The nocturnal buildup and strong negative gradient, the drawdown and gradient reversal after dawn, establishment of a steady positive gradient during the day, and reversal at dusk, can all be clearly seen.

Soil bacteria are an almost universal source of N_2O,[37] which is an important greenhouse gas and source of nitrogen oxides active in catalytic stratospheric ozone depletion. In typical natural and agricultural environments, fluxes per square metre are small, but when multiplied by large areas of the earth's surface are a dominant source of N_2O to the atmosphere.[1] The small fluxes and their variability in both time and space lead to large uncertainties in estimating the global N_2O source term in its atmospheric budget, and for this reason it is important to improve methods for estimating average N_2O source strengths over large areas. Figure 8(b) shows the diurnal variations in N_2O from the 1995 OASIS

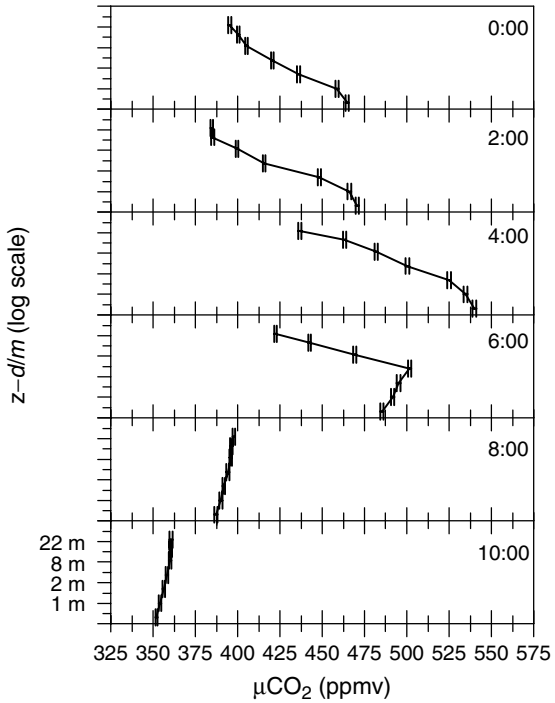

Figure 7. Vertical profiles of CO_2 above a rapidly growing lucerne grass crop (midnight – 10.00 am).

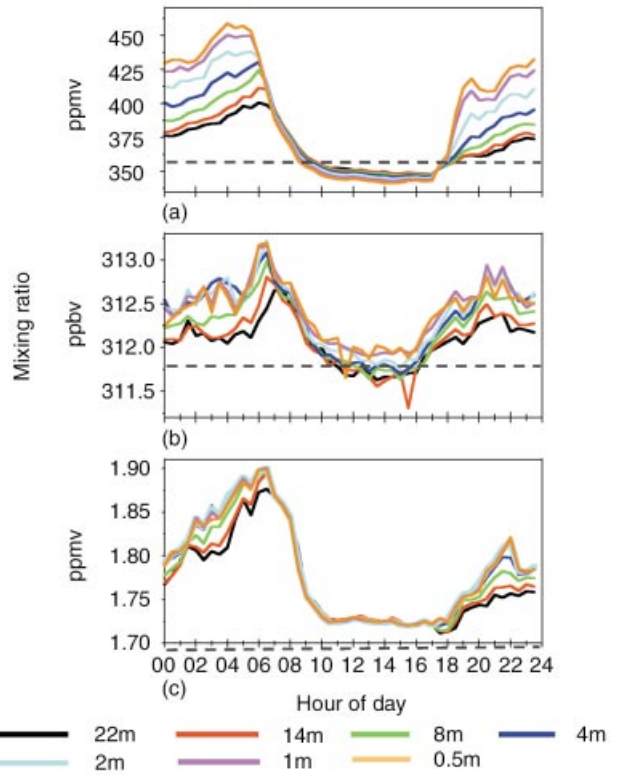

Figure 8. Average diurnal cycle of mixing ratios of trace gases at heights from 0.5 to 22 m above a rapidly growing lucerne crop: (a) CO_2; (b) N_2O; (c) CH_4.

campaign from which such estimates can be calculated. However the average top-to-bottom difference is less than 1 ppbv, which must be resolved against a background of around 310 ppbv in the surrounding air. High precision is thus required; the precision achieved here, ca. 0.2 ppbv per measurement, translates into a minimum detectable flux of ca. 20 ngN m^{-2} s^{-1}. The measured fluxes during OASIS 1995 were of approximately this magnitude. Earlier measurements from nitrogen-rich soils provided significantly higher fluxes.[8,33,35]

In the case of CH_4 (Figure 8c), the dominant regional source is from sheep and cattle. There is no significant source or sink of CH_4 in the area upwind contributing to the vertical gradients (ca. 200 m), which are therefore very small during the daytime and cannot be resolved with the 5 ppbv precision achieved. There is however a significant buildup in CH_4 in the nocturnal boundary layer, which effectively acts as an integrating volume to collect CH_4 emissions from the surrounding landscape, including the regional population of livestock. Under favorable circumstances, the rate of buildup in the nocturnal boundary layer can be used to infer the regional average CH_4 source strength.[38]

Figure 9 shows fluxes of ammonia, NH_3, released following application of liquid manure fertilizer to a young wheat crop.[8] In these measurements air was sampled continuously from inlets at three heights above the surface and analyzed pseudo-simultaneously by a dual beam FT-IR spectrometer in matched White cells with 96 m pathlength. Eddy diffusion coefficients were determined from measurements of the vertical profile of wind speed, and combined with the vertical concentration gradients to provide a flux measurement every 20 min automatically and continuously for several days following manure application. The detection limits for NH_3 were ca. 8 ppbv or 6 μg m^{-3} for concentrations, corresponding to fluxes of ca. 0.5 μg m^{-2} s^{-1}. The slow decrease in emission rate as the fertilizer load is processed by the soil and plants, and the diurnal cycle

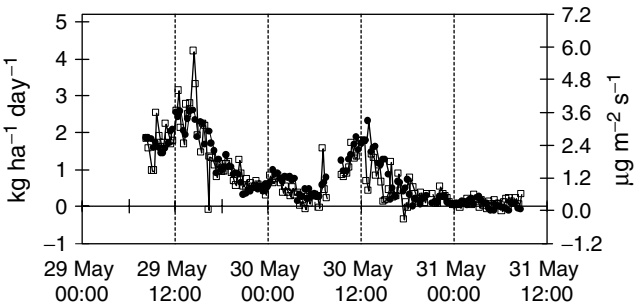

Figure 9. Fluxes of ammonia released from a young wheat crop after liquid manure fertilization, measured by the FT-IR flux gradient technique in Sweden 1993. [Reproduced by permission of Elsevier Science Ltd., from Griffith and Galle (2000).[8]]

Table 2. Precision of analyses and detection limits for trace gas fluxes using the FT-IR flux gradient method.

Species	Precision	Min. detectable flux
CO_2	1 ppmv	100 μg m^{-2} s^{-1}
CH_4	5 ppbv	120 ng m^{-2} s^{-1}
N_2O	0.2 ppbv	20 ng m^{-2} s^{-1}
NH_3	8 ppbv	500 ng m^{-2} s^{-1}

due to temperature and wind speed are clearly evident. A significant amount of fertilizer nitrogen is lost during and after application due to volatilization as NH_3, which is a notoriously difficult gas to measure routinely in the atmosphere in trace amounts. The FT-IR method represents a major advance in feasibility of following such nutrient losses.

These measurements serve to illustrate the utility of FT-IR-based analysis for micrometeorological flux measurements. With the existing equipment, approximate precisions in mixing ratios and lower limits to detectable fluxes are summarized in Table 2. Measurements of CO_2, CH_4, N_2O, CO and water vapor can be made simultaneously with a single spectrometer. NH_3 can be added to this suite if an MCT detector is used. To our knowledge the only other techniques reported for micrometeorological measurements of N_2O and CH_4 fluxes are based on eddy correlation or flux-gradient techniques using tunable diode laser spectrometers for analysis.[39–41] FT-IR is not suitable for eddy correlation measurements near the ground because of the high time resolution required (ca. 10 Hz).

3.2.2 Mass balance methods

Another approach to nonintrusive measurement of trace gas fluxes and emissions is based on a mass balance approach.[42,43] This approach is illustrated by measurements of CH_4 emissions from free-ranging sheep on a typical pasture.[44,45] The sheep are confined within a 22 × 22-m square open enclosure or fence, as illustrated in Figure 10. Air is sampled evenly and continuously along the full length of each side of the enclosure at heights of 0.5, 1, 2 and 3.5 m, through 40-L buffer volumes as described above to average out short-term fluctuations. The 16 air streams are analyzed sequentially at 2.8 min per stream by the dual beam FT-IR spectrometer in the same manner as described for flux gradient measurements, providing 45-min average concentrations in each inlet line. For each 45-min averaging period, the flux of CH_4 across each face of the enclosure is calculated as the integral of the mean concentration $\overline{C}_{CH_4}$ times the mean windspeed perpendicular to the face

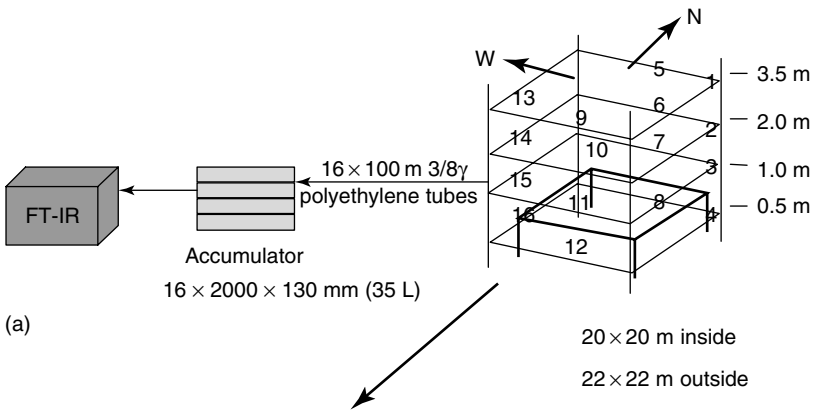

Figure 10. Illustration of the enclosure mass balance technique, in this example used for the nonintrusive measurement of CH_4 emissions from sheep.[45]

$\overline{U}$ at each height

$$F_{CH_4} = \int \overline{U} \cdot \overline{C}_{CH_4} \, dz \tag{3}$$

By mass balance, the difference between the fluxes across the two downwind faces and the two upwind faces must be due to emissions released within the enclosure. The upper level of 3.5 m is chosen to ensure that loss of emissions from the top of the enclosure is negligible unless the mean wind speed is very low. Figure 11 illustrates the differential horizontal flux densities $\overline{U} \cdot (\overline{C}_d - C_u)$ (where d is downwind and u is upwind) for four consecutive 45-min periods with 14 sheep in the enclosure, where the wind was predominantly north–south during the first three periods and veered to the SE during the 12 : 45 period. Integration of the vertical profiles and multiplication by the fence length provides the net CH_4 flux out of the enclosure, which is assumed to be due to the 14 sheep. The technique measured a mean emission rate of 11.9 ± 1.5 g CH_4 day^{-1} per sheep and was in excellent agreement with a totally independent method carried out simultaneously during the study.[44]

In this example, the strength of the FT-IR analysis is in the ability to measure the 16 air samples within a reasonable time, 45 min, suitable for averaging meteorological conditions, while still providing sufficient precision to resolve the small differences between the sample lines. FT-IR precision for CH_4 of ca. 5 ppbv was obtained for the 2.8-min cycle time, while typical downwind–upwind differences at the lower levels were a few tens of ppbv. Automation is also an important advantage, allowing continuous 24-h monitoring of the emissions and characterization of the diurnal variations and short-term changes due to animal behavior. N_2O and CO_2 emissions from the 24×24-m enclosure could also be retrieved from analysis of the collected spectra.

3.3 Tracer methods for estimating trace gas release rates from localized sources

Tracer methods are well suited to the quantification of emissions from localized sources.[46–48] They are based on the release of an inert tracer gas at the same location as the source of interest, and analysis of both species sufficiently

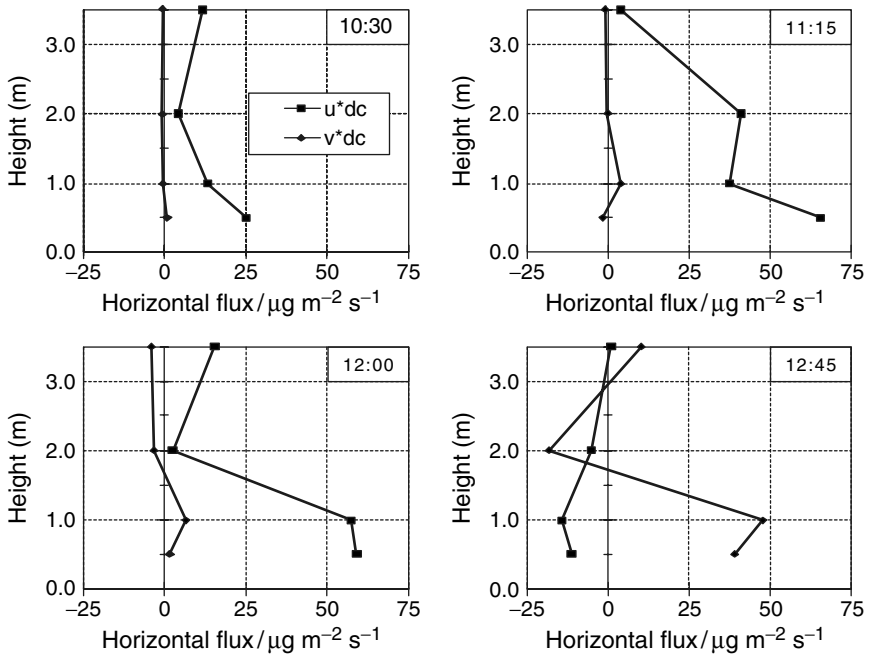

Figure 11. Vertical profiles of differential horizontal flux densities of CH_4 in the north–south and east–west directions of a 24 × 24 m fence enclosing 14 sheep. Integration over height provides the net fluxes out of the enclosure along the two directions. [Reproduced by permission of Elsevier Science Ltd., from Leuning *et al.* (1999).[44]]

downwind of the source that the tracer and target gas appear to come from the same location. In this case, if the tracer release rate F_T is known, the emission rate F_x of target gas x from the co-located source is simply calculated from the ratio of concentrations of the target gas, C_x and the tracer C_T:

$$F_x = F_T \frac{C_x}{C_T} \tag{4}$$

In this method, the tracer measurement essentially corrects for fluctuations in concentration of x brought about by variations in wind and transport of air parcels to the measurement site. The tracer gas should be inert, not be released by the source, have a low or at least constant mixing ratio in the background air, and be detectable in small quantities; SF_6 has commonly been used. N_2O can also be suitable provided there are no local sources since its concentration in background air, though high at 310 ppbv, is usually quite constant.

Galle, Mellqvist and co-workers have used the tracer method with trace gas analysis by FT-IR spectrometry to quantify industrial fugitive emissions[47,48] and CH_4 from landfills.[46] They employ both open path and closed cell FT-IR methods to measure both target gases and tracer gas in a single measurement. FT-IR allows real time continuous measurements, which adds considerably to the technique: if only a few measurements of trace gas ratios can be made, it is essential that there be no sources of the target gas other than those co-located with the tracer release. However a time series of measurements allows a time-correlation between target gas and tracer to isolate those emissions which are co-located with the tracer release. An additional approach can also be used to minimize the impact of variable winds and sources not co-located with the tracer gas release. If a weighted mean ratio of target to tracer gas concentration is taken, with the weights equal to the actual tracer amount (or its square), those periods where the wind does not blow from the tracer release areas will have low tracer amounts and will carry less weight in determining the mean.[47] Figure 12 shows such a time series of CH_4 and N_2O tracer mixing ratios downwind of a landfill site in which N_2O was released at known rates from cylinders located around the landfill. In this case the CH_4 and N_2O concentrations are well correlated at all times and from a regression of CH_4 against N_2O and the known N_2O release rate, a total CH_4 emission rate for the landfill can be calculated. Regular bimonthly measurements gave an annual average total emission rate of CH_4 of 37.5 kg h^{-1} or 330 tonnes yr^{-1} from the landfill.

We have used similar methods to estimate CH_4 emissions from cattle.[45,49] In this application, 30–80 head of yearling dairy cattle were confined in a 30 × 7-m area oriented across the wind direction 40 m upwind of a 6-m micrometeorological mast. N_2O tracer was released at a constant rate from 10 capillaries evenly spread along the upwind fence of the cattle enclosure. Air samples were

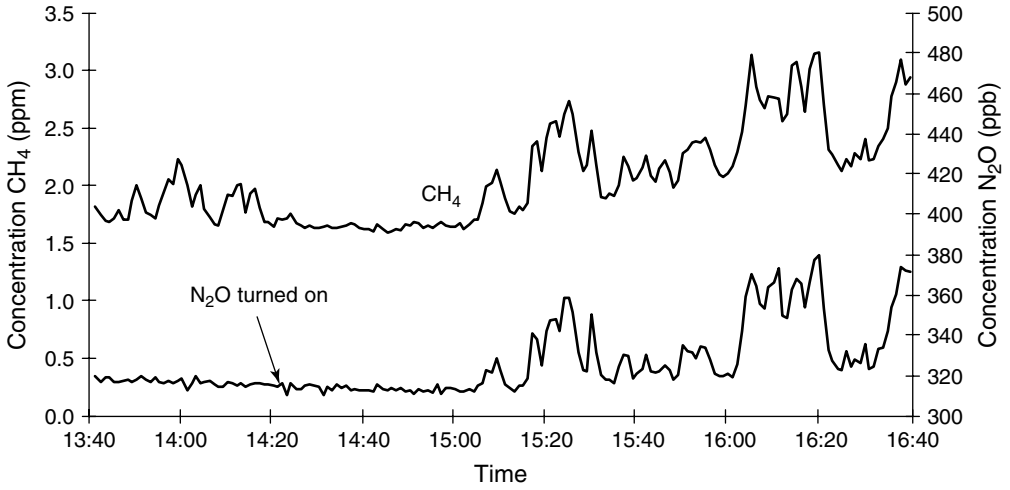

Figure 12. Time series of methane and nitrous oxide tracer emitted from a landfill site measured simultaneously downwind. [Courtesy of B. Galle, Chalmers Technical University, Gothenburg, Sweden.]

drawn continuously from inlets at four heights on the mast and analyzed sequentially by a single beam FT-IR spectrometer operating on a 5 min measurement cycle. Figure 13 illustrates the correlation between measured CH_4 and N_2O tracer concentrations. On three separate days we obtained very consistent average emissions of 370 ± 30 g or 460 ± 40 standard liters per day per head of cattle.

In summary, FT-IR spectroscopy has distinct advantages for tracer technique applications. These include simultaneous and continuous in situ determination of several target species, including common tracers such as SF_6 and N_2O with good sensitivity (low ppbv range) and good time resolution (minutes). This combination allows time-correlative analysis and enhances the power of tracer methods substantially over bag or flask-sampling based methods with laboratory-based trace gas analysis.

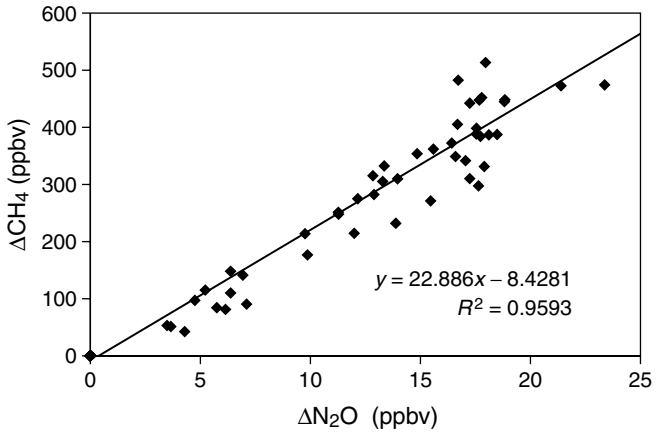

Figure 13. Correlation of CH_4 emissions from cattle and N_2O tracer downwind of a herd of 80 cattle. Plotted values are excesses over background levels.[45]

3.4 Field chamber measurements of trace gas exchange fluxes

The third but simplest approach to trace gas flux measurement is the use of flux chambers. In this approach, a (usually small) area of the surface is enclosed by an open-bottomed chamber, and from the rate of change of concentration of a trace gas in the chamber, the flux can be calculated from:

$$F_x = \frac{V}{A}\frac{\mathrm{d}C_x}{\mathrm{d}t} \tag{5}$$

where F_x and C_x are the flux and concentration of trace gas x, V is the chamber volume and A the area of surface enclosed. In normal practice small samples of air in the chamber are collected before closure and once or twice at a suitable time after closure for analysis by conventional techniques, typically for example by gas chromatography for N_2O and CH_4. Chambers have the advantages that they are relatively simple to deploy, and are able to resolve very small fluxes. However they suffer the major disadvantages that they perturb the system they are measuring by altering the microclimate, including light levels, temperature, humidity and atmospheric exchange, and they sample only small areas for typically a few minutes to an hour. To capture the well recognized spatial and temporal variability in emissions, many chambers must be employed, and be analyzed repetitively.

FT-IR spectroscopy can be used to carry out automated, in situ analysis of chamber air to reduce some of the disadvantages of the technique. During the 1995 OASIS campaign, we operated two field chambers coupled to a single beam FT-IR spectrometer and 22-m White cell continuously for the duration of the experiment.[50] The chambers were analyzed alternately on a 1-h cycle with

each chamber closed for 20 min in the middle of its 30-min analysis time. Air was circulated in a closed loop between the chamber being analyzed and the White cell in the spectrometer through $\frac{1}{2}''$ tubing and an oil-free diaphragm pump. Spectra were recorded continuously and saved every minute to provide time series of chamber concentrations of CO_2, N_2O and CH_4. All valve switching, pump and spectrometer control, chamber closure, data acquisition and spectrum analysis was fully automated by an Array Basic program. Fluxes were calculated in real time immediately after each closure. Figure 14 shows concentration changes during a typical 30-min measurement period, in which the chamber was closed after 5 min and reopened after 25 min. The emission rates of CO_2 and N_2O are determined from the slopes of the time series during the closed period, and correspond to 85 $gC\,m^{-2}\,s^{-1}$ and 9.6 $ngN\,m^{-2}\,s^{-1}$, respectively. From the scatter in the data of Figure 14(b), we estimate that small fluxes of N_2O of the order of 1 $ngN\,m^{-2}\,s^{-1}$ could be resolved with this system, substantially better than the limits available using micrometeorological methods. However the precision for CH_4 analysis (5 ppbv) was not sufficient to resolve any CH_4 fluxes, at least over 20-min closure times. Small uptake rates of around 5 $ng\,m^{-2}\,s^{-1}$ were measured by gas chromatographic analysis of closures averaged over 12-h periods.[50]

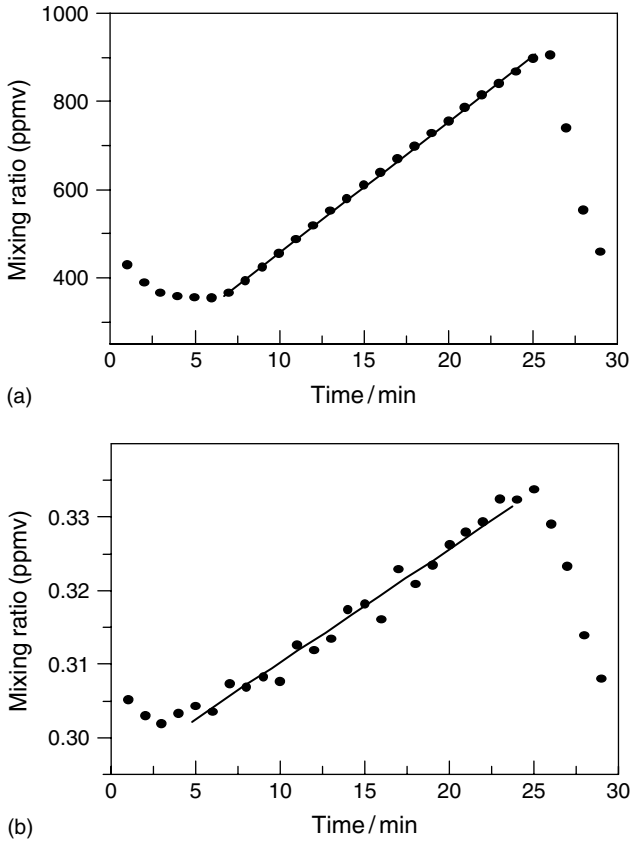

Figure 14. Thirty-minute time series of (a) CO_2 and (b) N_2O in a 100-L flux chamber covering 0.35 m^2 of surface. The chamber is closed 5 min and reopened 25 min after the start of the cycle. The emission rates of CO_2 and N_2O are determined from the slopes of the time series during the closed period, and correspond to 85 $g\,C\,m^{-2}\,s^{-1}$ and 9.6 $ng\,N\,m^{-2}\,s^{-1}$, respectively.

Automation also provided regular hourly determinations of the fluxes, so that diurnal and other short term variations in the fluxes could be observed. Figure 15 shows the hourly fluxes of CO_2 and N_2O for the duration of the 1995 OASIS campaign. The chambers were dark when closed, so that CO_2 fluxes are only due to respiration, not photosynthesis. They follow a clear diurnal cycle related to temperature, and the mean respiration rate over the period was 98 $\mu gC\,m^{-2}\,s^{-1}$. N_2O also shows a distinct diurnal cycle, but the record is dominated by pulses of emission following minor and major rainfall events on 13 and 21 October respectively. N_2O emission is regulated to a large extent by soil moisture, and with strong emissions after rain decaying over a period of 2–3 days as the soil dries out. The results are analyzed in more detail by Meyer *et al*.[50] Galle *et al*.[51] describe similar, longer-term automated chamber measurements of CO_2 and N_2O from an organic soil.

Galle *et al*.[33] also first described the use of an ultra-large chamber with FT-IR analysis to improve spatial averaging of emission measurements. In this work, the chamber was

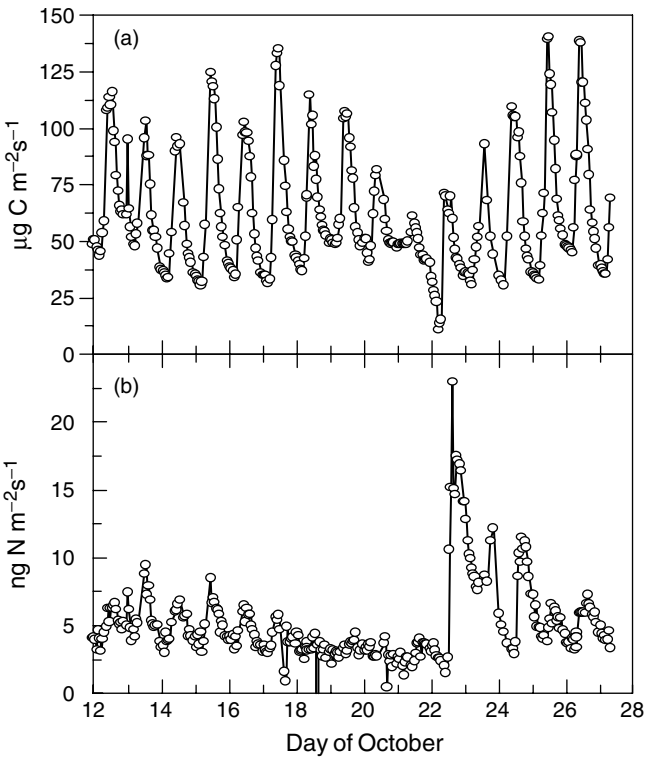

Figure 15. Hourly fluxes of (a) CO_2 and (b) N_2O for 2 weeks of the 1995 OASIS campaign.

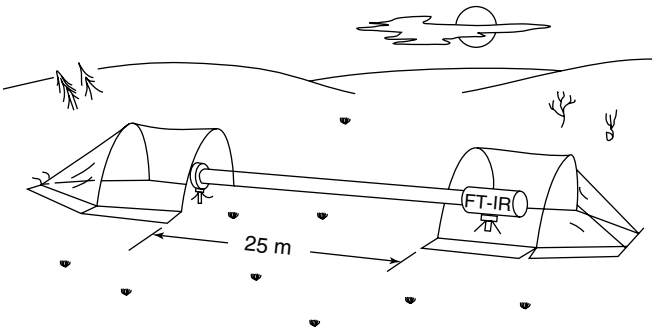

Figure 16. Ultra large chamber for spatially averaged flux measurements. [Reproduced by permission of the American Geophysical Union, from Galle *et al*. (1994).[33]]

an elongated nylon tunnel tent ca 30 m long and 2 m wide (Figure 16). The tent enclosed an open path, 25-m base, 40-pass multiple reflection optical cell with 1 km total optical path,[52] directly coupled to an FT-IR spectrometer also inside the tent. Open path spectra were recorded continuously before, during and after closure of the tent and provided excellent sensitivity for emissions and uptake of N_2O and CH_4 in agricultural and forest soils.[35,53]

FT-IR analysis can thus alleviate some of the disadvantages of chamber methods to some extent. Firstly, through automated in situ analysis, repetitive measurements are relatively easy to carry out for temporal averaging, and an array of many fully automated chambers may be envisaged to provide better spatial averaging. Secondly, fluxes can be determined with high time resolution to resolve diurnal and other short term variations in fluxes. Finally, CO_2, N_2O and CH_4 fluxes can be determined simultaneously with a single instrument, with flux detection limits of ca. $1\,\mathrm{ngN\,m^{-2}\,s^{-1}}$ for N_2O and $5-10\,\mathrm{ngC\,m^{-2}\,s^{-1}}$ for CH_4. Detection limits are more than adequate for CO_2 flux measurements.

3.5 $^{13}CO_2$ fractionation during plant respiration

Natural variations in isotopic abundances come about because (bio)chemical reaction rates and equilibrium constants depend on molecular mass and the distribution of molecular energy levels. Isotopic variations in atmospheric gases thus provide a very valuable diagnostic for the processes which create, destroy and transform those gases.[54] Isotope ratio mass spectrometry (IRMS) is normally employed for isotopic analysis, but IR spectrometry is also suitable since different isotopomers have different vibrational and rotational frequencies. Since the isotopic fractionations of interest are often small, of the order of 1‰ (i.e. 0.1%) or less, high precision is required.

The ν_3 absorption band of $^{13}CO_2$ is shifted by $66\,\mathrm{cm^{-1}}$ to a lower wavenumber than the corresponding band of $^{12}CO_2$, and is thus easily resolvable at $1\,\mathrm{cm^{-1}}$ resolution.

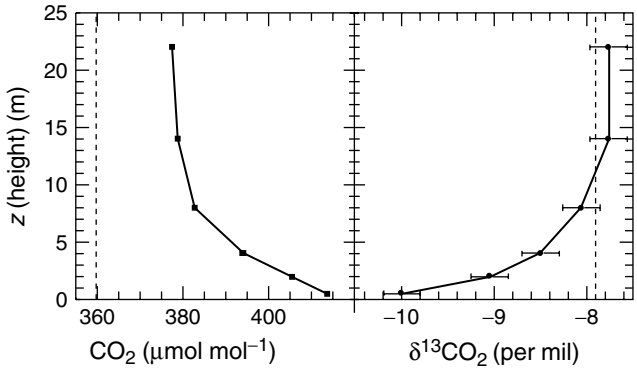

Figure 17. Simultaneous CO_2 and $\delta^{13}CO_2$ vertical profiles over a spring pasture at 22 : 30, October 1995. See text for discussion. [Reproduced by permission of the American Chemical Society, from Esler *et al*. (2000).[55]]

This provides the basis for FT-IR measurements of ^{13}C fractionation in CO_2. As a demonstration of the capabilities, during the OASIS measurement campaign in 1995 (Section 3.2.1) we analyzed vertical profiles of $^{13}CO_2$ and $^{12}CO_2$ from 0.5 to 22 m above ground from the micrometeorological tower.[55] Figure 17 illustrates such a profile at 22 : 30 over spring pasture, where plant and soil respiration creates a strong vertical gradient (decreasing upwards) in CO_2 and a corresponding profile of the ^{13}C fractionation, $\delta^{13}CO_2$. Isotope ratios are normally expressed in relative "per mil" units relative to an accepted standard:

$$\delta^{13}\mathrm{C} = \left(\frac{R^{13}_{\mathrm{sample}}}{R^{13}_{\mathrm{standard}}} - 1 \right) \times 1000$$

where $R^{13} = {}^{13}\mathrm{C}/{}^{12}\mathrm{C}$ is the ratio of abundances of ^{13}C and ^{12}C. The precision of $\delta^{13}CO_2$ determination is approximately 0.2‰. Plant photosynthesis discriminates against ^{13}C, so that plant organic material is isotopically lighter in ^{13}C than atmospheric CO_2. When plant carbon is oxidized during respiration, the respired CO_2 carries the isotopic signature of the plant carbon. A plot of $\delta^{13}CO_2$ vs $1/[CO_2]$[56] should have a Y- intercept equal to the ^{13}C isotopic signature of the plant CO_2; such a plot is shown in Figure 18 and has an intercept of -25.7 ± 0.8‰, typical of that expected from plants of this type.

Conventional IRMS normally requires collection of a sample, with return to a central laboratory for analysis. Sample throughput is limited. While the FT-IR technique does not attain the very high precision available with IRMS (<0.1‰), the above measurements demonstrate the possibility of field-based, in situ analysis of isotope ratios. The technique opens up the possibility of much more intensive field measurements, allowing many samples to be measured in near-real time, short-term changes and diurnal cycles to be characterized, and process studies to be carried out in much more detail.

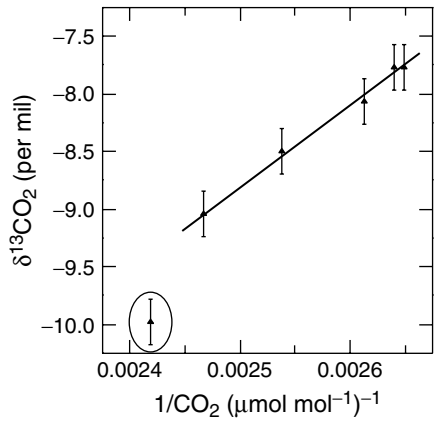

Figure 18. $\delta^{13}CO_2$ vs inverse CO_2 mixing ratio for the data of Figure 17. The regression line excludes the circled outlier. [Reproduced by permission of the American Chemical Society, from Esler *et al*. (2000).[55]]

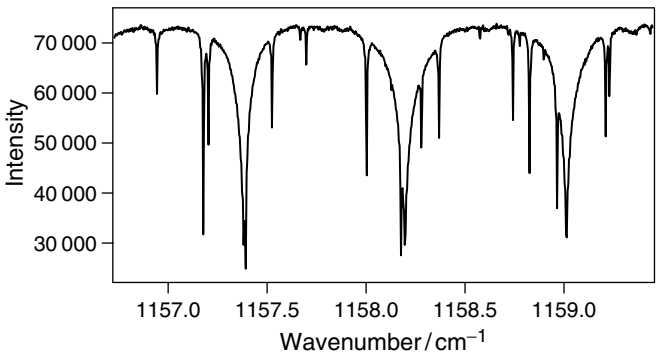

Figure 19. Section of a ground-based solar FT-IR spectrum near 1156 cm^{-1} illustrating the lineshape dependence on the vertical distribution of the absorber. The three broader lines are due to N_2O, which resides predominantly in the troposphere, and the narrow lines are due to ozone, most of which is in the stratosphere.

4 GROUND-BASED SOLAR FT-IR REMOTE SENSING

The sun is a very good radiation source, with an effective black body temperature of 5800 K and an angular size large enough to overfill the field of view of a typical FT-IR optical system. When spectra of the sun are recorded through the atmosphere, rich spectra with high S/N and high spectral resolution can be obtained in a few seconds to minutes. Remote sensing of atmospheric composition by solar IR spectroscopy is routinely carried out from the ground, aircraft, high altitude balloons and from space. Beer[57] and Rao and Weber[58] provide a detailed introduction to FT-IR remote sensing and atmospheric spectroscopy.

Atmospheric pressure drops off approximately exponentially with altitude; the total vertical atmospheric column at sea level is equivalent to that of a single layer 8-km thick at 1 atm pressure and 273 K, and increases approximately as the secant of the solar zenith angle. In the lower atmosphere individual spectral lines are predominantly pressure broadened with near-Lorentzian lineshapes and pressure-dependent widths, whereas in the upper atmosphere pressure broadening is dominated by Doppler broadening and the lineshapes are predominantly Gaussian and dependent on temperature but not pressure. Thus atmospheric solar spectra display lineshapes that depend on the altitude range of the light path and vertical distribution of the absorber molecules in the atmosphere. Figure 19 illustrates this effect, with a portion of the solar spectrum measured at 0.004 cm^{-1} resolution near 1150 cm^{-1}. The broader lines are due to N_2O, which resides predominantly in the troposphere (<15 km altitude), and the narrow lines are due to ozone, most of which is in the stratosphere (>20 km). Quantitative analysis of solar FT-IR spectra is normally carried out by NLLS fitting of calculated spectra (see for example Section 2.3) to measured spectra. The equivalent width of each line (i.e. the area under the line) is related to the total column amount of the absorbing species, and detailed analysis of the lineshape provides a method for retrieving limited information on the vertical distribution.[13,59,60]

For ground-based solar FT-IR spectrometry, a sun tracker is used to image the solar disk onto the entrance aperture of the FT-IR spectrometer, which normally has high resolution (0.004 cm^{-1}) to resolve the lineshapes of stratospheric gases and provide some altitude resolution. MCT detectors are normally used below 1800 cm^{-1} and InSb detectors above 1800 cm^{-1}, with optical bandpass filters usually required to reduce the total flux on the detector and avoid detector saturation. Single scans typically provide S/N of 200–1000 at high resolution. Despite its much lower intensity as a radiation source, the moon has also been used as a source for atmospheric measurements in the high Arctic.[61] A global network of ground-based solar FT-IR stations operates as a part of the Network for Detection of Stratospheric Change (NDSC, http://www.ndsc.ncep.noaa.gov/).[62] Atmospheric constituents that can be detected include ozone (four different isotopomers), major chlorine and fluorine species (HCl, $ClONO_2$, HF and COF_2), species related to ozone destruction including ClO, HNO_3, NO, NO_2, halocarbons such as CFC-11, CFC-12 and CFC-22, major greenhouse gases such as CO_2, H_2O, HDO, CH_4, N_2O, and a number of other mainly tropospheric species including C_2H_2, C_2H_4, C_2H_6, CO, H_2CO, HCN, HO_2NO_2, NH_3, OCS and SO_2. For further details we refer the reader to a sample of publications from some of the NDSC groups.[59,60,63–70]

Ground-based solar spectroscopy can be carried out from any altitude but is best from higher altitudes to reduce absorption by water vapor (which is heavily concentrated near the ground) and undesirable effects of

pollution in the atmospheric boundary layer. Thus two of the best sites are at Mauna Loa in Hawaii (3400 m above sea level)[64] and the Jungfraujoch in Switzerland (3580 m above sea level).[67] Solar FT-IR spectroscopy from aircraft[71–73] and balloons[74–76] provide more detailed data on the upper atmosphere. For spectra collected with the sun above the observation altitude (zenith angles $<90^\circ$), the principles are the same as for ground-based measurements. For spectra collected near sunrise or sunset with the solar zenith angle below the observation altitude ($>90^\circ$), absorption is dominated by the atmospheric layers nearest the tangent altitude of the solar beam. An "onion-peeling" technique can then be used to determine vertical profiles, in which spectra are measured as the sun sets (or rises), and the spectra of upper layers are analyzed first and the analyses successively subtracted from those of the lower layers. Measurements can be made from up to 40 km altitude with large stratospheric balloons.

Satellite-borne FT-IR solar absorption spectrometers effectively observe from above the entire atmosphere and can provide pseudo-global coverage of atmospheric composition. For example the ATMOS spectrometer, which made several flights on the Space Shuttle in the 1980s and 1990s, has provided a large body of atmospheric composition data with broad geographic coverage. ATMOS typically measures 100 spectra at $0.017\,cm^{-1}$ resolution (60-cm OPD) during each 4-min solar occultation from the 300-km altitude orbit of the Space Shuttle; in the November 1994 mission, it measured 190 such occultations. For an overview and further details, see Gunson *et al.*[77] and following papers in a special issue of *Geophysical Research Letters*. A number of other satellite-borne FT-IR spectrometers have already been flown, with many more planned for the next few years.

5 CONCLUSIONS

We have described FT-IR spectrometry as a technique for the analysis of trace gases in air. The techniques have a number of advantages including:

- simultaneous determination of CO_2, CO, CH_4 and N_2O at clean air levels, as well as natural variations in the $^{13}CO_2/^{12}CO_2$ ratio;
- high precision and accuracy, of the order of 0.1% for CO_2, N_2O and CH_4, 0.5% for CO and 0.1‰ for $^{13}CO_2/^{12}CO_2$;
- portability, reliability and automation for long term measurements in field experiments;
- cost effectiveness, able to determine several gases with a single instrument.

Applications include both "simple" composition measurements as well as several methods for measuring the fluxes of trace gases between the atmosphere and sources and sinks at the earth's surface. Although our focus has been on clean air and the global atmosphere, the methods are equally applicable to polluted air analysis for a wide range of species, typically with low parts per billion detection limits.

ACKNOWLEDGMENTS

I am very grateful to acknowledge the students and colleagues who have contributed to the body of work described here and without whom it would not have happened. These include Michael Esler, Ian Jamie, David Hsu, Fred Turatti, Paul Beasley and Stephen Wilson of the University of Wollongong, Bo Galle at Chalmers University of Technology, Sweden, Ray Leuning, Tom Denmead, Mick Meyer and Ian Galbally of CSIRO, Australia, Andy Reisinger of NIWA, NZ, the staff of the Cape Grim station in Tasmania, and many others who made the many field trips possible.

ABBREVIATIONS AND ACRONYMS

IRMS	Isotope ratio mass spectrometry
NDSC	Network for Detection of Stratospheric Change
NIST	National Institute for Standards and Technology
NLLS	Nonlinear Least Squares

REFERENCES

1. IPCC, 'Climate Change 1995: The Science of Climate Change', Cambridge University Press, Cambridge (1996).
2. D.W.T. Griffith and I.M. Jamie, 'Fourier Transform Infrared Spectrometry in Atmospheric and Trace Gas Analysis', in "Encyclopedia of Analytical Chemistry", ed. R.A. Meyers, Wiley, Chichester, 1979–2007 (2000).
3. M.B. Esler, D.W.T. Griffith, S.R. Wilson and L.P. Steele, *Anal. Chem.*, **72**(1), 206 (2000).
4. M.B. Esler, PhD thesis, University of Wollongong, Wollongong (1997).
5. J.U. White, *J. Opt. Soc. Am.*, **32**, 285 (1942).
6. J.U. White, *J. Opt. Soc. Am.*, **66**, 411 (1976).
7. D. Horn and G.C. Pimentel, *Appl. Opt.*, **10**, 1892 (1971).
8. D.W.T. Griffith and B. Galle, *Atmos. Environ.*, **34**, 1087 (2000).
9. D.W.T. Griffith, R.L. Leuning, O.T. Denmead and I.M. Jamie, *Atmos. Environ.*, submitted.

10. R.J. Anderson and P.R. Griffiths, *Anal. Chem.*, **47**(14), 2339 (1975).
11. C. Zhu and P.R. Griffiths, *Appl. Spectrosc.*, **52**(11), 1403 (1998).
12. C. Zhu and P.R. Griffiths, *Appl. Spectrosc.*, **52**(11), 1409 (1998).
13. D.W.T. Griffith, *Appl. Spectrosc.*, **50**(1), 59 (1996).
14. L.S. Rothman, C.P. Rinsland, A. Goldman, S.T. Massie, D.P. Edwards, J.M. Flaud, A. Perrin, C. Camypeyret, V. Dana, J.Y. Mandin, J. Schroeder, A. Mccann, R.R. Gamache, R.B. Wattson, K. Yoshino, K.V. Chance, K.W. Jucks, L.R. Brown and V. Nemtchinov, *J. Quant. Spectrosc. Radiat. Transfer*, **60**, 665 (1998).
15. J.W. Brault, 'Fourier Transform Spectroscopy', in "High Resolution in Astronomy", eds A. Benz, M. Huber and M. Mayor, Geneva Observatory, 1–62 (1985).
16. R.J. Bell, 'Introduction to Fourier Transform Spectroscopy', Academic Press, New York (1972).
17. J. Kauppinen and P. Saarinen, *Appl. Opt.*, **31**(1), 69 (1992).
18. P. Saarinen and J. Kaupinnen, *Appl. Opt.*, **31**(13), 2353 (1992).
19. D.M. Haaland, 'Multivariate Calibration Methods Applied to Quantitative FTIR Analyses', in "Practical Fourier Transform Infrared Spectroscopy", eds J.R. Ferraro and K. Krishnan, Academic Press, San Diego, 395–468 (1990).
20. D.M. Haaland, R.G. Easterling and D.A. Vopika, *Appl. Spectrosc.*, **39**, 73 (1985).
21. D.M. Haaland and D. Melgaard, *Appl. Spectrosc.*, **54**(9), 1303 (2000).
22. C.L. Lin, E. Niple, J.H. Shaw and J.G. Calvert, *Appl. Spectrosc.*, **33**(5), 481 (1979).
23. E. Niple, *Appl. Opt.*, **19**(20), 3481 (1980).
24. P.R. Bevington, 'Data Analysis and Error Analysis for the Physical Sciences', McGraw-Hill, New York (1969).
25. W.H. Press, S.A. Teukolsky, W.T. Vetterling and B.P. Flannery, 'Numerical Recipes in Fortran: The Art of Scientific Computing', 2nd edition, Cambridge University Press, Cambridge (1992).
26. R.J. Francey, L.P. Steele, R.L. Langenfels, M.P. Lucarelli, C.E. Allison, D.J. Beardsmore, S.A. Coram, N. Derek, F.R.d. Silva, D.M. Etheridge, P.J. Fraser, R.J. Henry, B. Turner, E.D. Welch, D.A. Spencer and L.N. Cooper, 'Global Atmospheric Sampling Laboratory (GASLAB)', in "Baseline Atmospheric Program Australia 1993", eds R.J. Francey, A.L. Dick and N. Derek, Bureau of Meteorology, CSIRO Division of Atmospheric Research, Melbourne, 8–29 (1996).
27. D.W.T. Griffith and M.B. Esler, in preparation.
28. D.W.T. Griffith, M.B. Esler and I.M. Jamie, 'Improved Accuracy of FTIR Gas Analysis using Synthetic Calibration Spectra', Presented at 3rd Australian Conference on Vibrational Spectroscopy (1998).
29. J.L. Gras, N. Derek, N.W. Tindale and A.L. Dick (eds), 'Baseline Atmospheric Program Australia 1996', Bureau of Meteorology, Australia and CSIRO Atmospheric Research, Melbourne (1999).
30. G.P. Livingstone and G.L. Hutchinson, 'Enclosure-based Measurements of Trace Gas Exchange: Applications and Sources of Error', in "Biogenic Trace Gases: Measuring Emissions from Soil and Water", eds P.A. Matson and R.C. Harriss, Blackwell Science, Oxford, 14–51 (1995).
31. D.H. Lenschow, 'Micrometeorological Techniques for Measuring Biosphere–Atmosphere Trace Gas Exchange', in "Biogenic Trace Gases: Measuring Emissions from Soil and Water", eds P.A. Matson and R.C. Harriss, Blackwell Science, Oxford, 126–163 (1995).
32. J.L. Monteith and M.H. Unsworth, 'Principles of Environmental Physics', Edward Arnold, London (1990).
33. B. Galle, L. Klemedtsson and D.W.T. Griffith, *J. Geophys. Res.*, **99**(D8), 16 575 (1994).
34. K.J. Hargreaves, F.G. Wienhold, L. Klemedtsson, J.R.M. Arah, I.J. Beverland, D. Fowler, B. Galle, D.W.T. Griffith, U. Skriba, K.A. Smith, M. Welling and G.W. Harris, *Atmos. Environ.*, **30**(10–11), 1563 (1996).
35. S. Christensen, P. Ambus, J.R.M. Arah, H. Clayton, B. Galle, D.W.T. Griffith, K.J. Hargreaves, L. Klemedtsson, A.-M. Lind, M. Maag, A. Scott, U. Skriba, K.A. Smith, M. Welling and F.G. Wienhold, *Atmos. Environ.*, **30**(24), 4183 (1996).
36. M. Raupach, M.R. Raupach, R. Leuning, H.A. Cleugh, P.A. Coppin, O.T. Denmead, F.X. Dunin, G.D. Farquhar, I.E. Galbally, D.W.T. Griffith, L.M. Hacker, J. Lloyd, K.G. McNaughton and W. Reyenga, 'OASIS Science Plan (Observations at Several Interacting Scales). Investigations of the Biosphere–Atmosphere Exchanges of Energy, Water, CO_2, Trace Gases and Stable Isotopes in Heterogeneous Terrain at Scales from Leaf to Region', Technical Report no. 68, CSIRO Centre for Environmental Mechanics (1994).
37. M.K. Firestone and E.A. Davidson, 'Microbiological Basis of NO and N_2O Production and Consumption in Soil', in "Exchange of Trace Gases between Terrestrial Ecosystems and the Atmosphere", eds M.O. Andreae and D.S. Schimel, Wiley, New York, 7–21 (1989).
38. O.T. Denmead, R. Leuning, D.W.T. Griffith and C.P. Meyer, 'Some Recent Developments in Trace Gas Flux Measurement Techniques', in "Approaches to Scaling of Trace Gas Fluxes in Ecosystems", ed. A.F. Bouwman, Elsevier, Amsterdam, 67–84 (1999).
39. F.G. Wienhold, H. Frahm and G.W. Harris, *J. Geophys. Res.*, **99**(D8), 16 557 (1994).
40. C. Wagner-Riddle, G.W. Thurtell, G.K. Kidd, E.G. Beauchamp and R. Sweetman, *Can. J. Soil Sci.*, **77**, 135 (1997).
41. C.E. Kolb, J.C. Wormhoudt and M.S. Zahniser, 'Recent Advances in Spectroscopic Instrumentation for Measuring Stable Gases in the Natural Environment', in "Biogenic Trace Gases: Measuring Emissions from Soil and Water", eds P.A. Matson and R.C. Harriss, Blackwell Science, Oxford, 259–290 (1995).
42. O.T. Denmead, R. Leuning, L.A. Harper, R.R. Sharpe, J.R. Freney and D.W.T. Griffith, *Atmos. Environ.*, **32**(21), 3679 (1998).
43. O.T. Denmead, R. Leuning, D.W.T. Griffith, I.M. Jamie, M.B. Esler, L.A. Harper and J.R. Freney, *Boundary-Layer Meteorol.*, **96**(1–2), 187 (2000).

44. R. Leuning, S.K. Baker, I.M. Jamie, C.H. Hsu, L. Klein, O.T. Denmead and D.W.T. Griffith, *Atmos. Environ.*, **33**(9), 1357 (1999).
45. C.H. Hsu, PhD thesis, University of Wollongong, Wollongong (2001).
46. B. Galle, J. Samuelsson, B.H. Svensson and G. Borjesson, *Environ. Sci. Technol.*, **35**(1), 21 (2001).
47. J. Mellqvist, 'Application of Infrared and UV-visible Sensing Techniques for Studying the Stratosphere and for Estimating Anthropogenic Emissions'. PhD thesis, Chalmers University of Technology, Gothenburg (1999).
48. J. Mellqvist, D.W. Arlander, B. Galle and B. Bergqvist, 'Measurements of Industrial Fugitive Emissions by the FTIR Tracer Method (FTM)', Swedish Environmental Research Institute, Gothenburg (1996).
49. D. Hsu, D.W.T. Griffith and A.R. Reisinger, in preparation (2001).
50. C.P. Meyer, I.E. Galbally, Y. Wang, I.A. Weeks, I. Jamie and D.W.T. Griffith, 'Two Automatic Chamber Techniques for Measuring Soil–Atmosphere Exchanges of Trace Gases and Results of their use in the OASIS Field Experiment', CSIRO Atmospheric Research Technical Paper No. 51, CSIRO, Melbourne (2001).
51. B. Galle, P. Weslien, J. Samuelsson, A. Kasimir-Klemedtsson and L. Klemedtsson, *Eur. J. Soil Sci.*, submitted (2000).
52. D. Ritz, M. Hausmann and U. Platt, 'An Improved Open Path Multireflection Cell for the Measurement of NO_2 and NO_3', in "Proceedings of the Society for Photooptical and Instrumentation Engineers", eds H.I. Schiff and U. Platt, Society for Photooptical and Instrumentation Engineers, 200–211, Vol. 1715 (1993).
53. A. Priemé, S. Christensen, B. Galle, L. Klemedtsson and D.W.T. Griffith, *Atmos. Environ.*, **30**(9), 1375 (1996).
54. J.A. Kaye, *Rev. Geophys.*, **28**(8), 1609 (1987).
55. M.B. Esler, D.W.T. Griffith, S.R. Wilson and L.P. Steele, *Anal. Chem.*, **72**(1), 216 (2000).
56. C.D. Keeling, *Geochim. Cosmochim. Acta*, **13**, 322 (1958).
57. R. Beer, 'Remote Sensing by Fourier Transform Infrared Spectrometry', Wiley, New York (1992).
58. K.N. Rao and A. Weber (eds), 'Spectroscopy of the Earth's Atmosphere and Interstellar Medium', Academic Press, San Diego (1992).
59. X. Liu, F.J. Murcray, D.G. Murcray and J.M. Russell, *J. Geophys. Res.-Atmos.*, **101**(D6), 10175 (1996).
60. C.P. Rinsland, N.B. Jones, B.J. Connor, J.A. Logan, N.S. Pougatchev, A. Goldman, F.J. Murcray, T.M. Stephen, A.S. Pine, R. Zander, E. Mahieu and P. Demoulin, *J. Geophys. Res.*, **103**(D21), 28197 (1998).
61. J. Notholt, *J. Geophys. Res.-Atmos.*, **99**(D2), 3607 (1994).
62. M.J. Kurylo, 'Network for the Detection of Stratospheric Change', in "Proceedings of the Society for Photooptical and Instrumentation Engineers", eds J.L. McElroy and R.J. McNeal, Society for Photooptical and Instrumentation Engineers, 169–174, Vol. 1491 (1991).
63. G.P. Adrian, T. Blumenstock, H. Fischer, L. Gerhardt, T. Gulde, H. Oelhaf, P. Thomas and O. Trieschmann, *Geophys. Res. Lett.*, **18**(4), 783 (1991).
64. A. Goldman, F.J. Murcray, F.H. Murcray, R.D. Blatherwick and D.G. Murcray, *J. Geophys. Res.*, **93**, 12607 (1988).
65. D.W.T. Griffith, N.B. Jones and W.A. Matthews, *J. Geophys. Res.*, **103**(D7), 8447 (1998).
66. B. Galle, J. Mellqvist, D.W. Arlander, I. Floisand, M.P. Chipperfield and A.M. Lee, *J. Atmos. Chem.*, **32**(1), 147 (1999).
67. E. Mahieu, R. Zander, L. Delbouille, P. Demoulin, G. Roland and C. Servais, *J. Atmos. Chem.*, **28**(1–3), 227 (1997).
68. J. Notholt, A. Meier and S. Peil, *J. Atmos. Chem.*, **20**(3), 311 (1995).
69. N.B. Jones, M. Koike, W.A. Matthews and B.M. McNamara, *Geophys. Res. Lett.*, **21**(7), 593 (1994).
70. R. Sussmann and K. Schaefer, *Appl. Opt.*, **36**(3), 735 (1997).
71. W.G. Mankin, *Opt. Eng.*, **17**(1), 39 (1978).
72. G.C. Toon, C.B. Farmer, L.L. Lowes, P.W. Schapper, J.-F. Blavier and R.H. Norton, *J. Geophys. Res.*, **94**(D14), 16 571 (1989).
73. M.T. Coffey, W.G. Mankin and A. Goldman, *J. Geophys. Res.*, **86**(C8), 7331 (1981).
74. F.J. Murcray, J.J. Kosters, R.D. Blatherwick, J. Olson and D.G. Murcray, *Appl. Opt.*, **29**(10), 1520 (1990).
75. B. Sen, G.C. Toon, J.F. Blavier, E.L. Fleming and C.H. Jackman, *J. Geophys. Res.-Atmos.*, **101**(D4), 9045 (1996).
76. A. Goldman, R.D. Blatherwick, F.J. Murcray and D.G. Murcray, *Appl. Opt.*, **35**(16), 2821 (1996).
77. M.R. Gunson, M.M. Abbas, M.C. Abrams, M. Allen, L.R. Brown, T.L. Brown, A.Y. Chang, A. Goldman, F.W. Irion, L.L. Lowes, E. Mahieu, G.L. Manney, H.A. Michelsen, M.J. Newchurch, C.P. Rinsland, R.J. Salawitch, G.P. Stiller, G.C. Toon, Y.L. Yung and R. Zander, *Geophys. Res. Lett.*, **23**(17), 2333 (1996).